The Astronomical Journal, 151:124 (8pp), 2016 May doi:10.3847/0004-6256/151/5/124

NEAR-CONTACT BINARIES IZ MONOCEROTIS AND AR DRACONIS

Yuan-Gui Yang[1,2], Hai-Feng Dai[1,2], Zheng Zhou[1], and Qun Li[1]
[1] School of Physics and Electronic Information/Information College, Huaibei Normal University, Huaibei 235000, China; yygcn@163.com, yangyg@chnu.edu.cn
[2] Key Laboratory for the Structure and Evolution of Celestial Objects, Chinese Academy of Sciences, Kunming 650011, China
Received 2015 August 24; accepted 2016 February 22; published 2016 April 26

ABSTRACT

We present multi-color photometric observations for two neglected near-contact binaries, IZ Mon ($P = 0^{d}.77980$) and AR Dra ($P = 0^{d}.67584$). By the aid of the updated W-D analysis code, the photometric solutions were deduced from the multi-color light curves (LCs). IZ Mon is a semi-detached binary with a mass ratio of $q = 0.388(\pm0.002)$, while AR Dra is a detached star with a mass ratio of $q = 0.652(\pm0.002)$. The asymmetric LCs of IZ Mon were modeled by a hot spot on the secondary's surface, which may be attributed to mass transfer from the primary. Based on all collected eclipse times for two systems, we constructed their timing residual curves. The orbital period for IZ Mon may be continuously decreasing at a rate of $dP/dt = -2.06(\pm0.04)$ days yr^{-1}, which may result from mass and angular momentum loss from the central system. For AR Dra, there exists a cyclic variation with a period of $P_3 = 104.9(\pm2.9)$ yr due to light-time orbit effect via the presence of the third body, whose mass is more than $0.28(\pm0.02)\ M_{\odot}$. Finally, two near-contact binaries, IZ Mon and AR Dra, will evolve into contact binaries.

Key words: binaries: close – binaries: eclipsing – stars: individual (AR Dra, IZ Mon)

Supporting material: machine-readable tables

1. INTRODUCTION

Hoffmeister (1944) found IZ Mon (=AN 239.1964; $\alpha_{2000.0} = 06^{h}58^{m}01^{s}.05$ and $\delta_{2000.0} = 08°53'20''.1$) as a variable star, whose coordinations were identified by Kinnunen & Skiff (2000). It was classified to be an EB-type binary, whose visual magnitude is from $11^{m}.90$ to $12^{m}.60$ (Kukarkin et al. 1971). An orbital period for this star was determined to be $0^{d}.7798$, which was refined to be $0^{d}.779798$ (Kreiner 2004). From 32 low-precision light minimum times, Wood & Forbes (1963) derived a cubic ephemeris of Min.I = HJD 2433282.90241 + $0.7798490E + 1.21 \times 10^{-8}E^2 + 9.83 \times 10^{-13}E^3$. Although some eclipsing times were monitored in literature, no photoelectric/CCD light curves (LCs) have been published up to now.

AR Dra (=BV 226; $\alpha_{2000.0} = 12^{h}16^{m}36^{s}.563$ and $\delta_{2000.0} = 64°51'27''.57$) was discovered by Strohmeier (1959a). Its color index is $B - V = +0.53$ (Koch 1974). Hill et al. (1975) gave a spectral type of F5V. Based on photographic eclipsing times, Strohmeier (1959b) determined a period of $0^{d}.675839$, which was subsequently improved to be $0^{d}.67583575$ (Broglia & Conconi 1979), $0^{d}.67583743$ (Kreiner et al. 2001), and $0^{d}.6758397$ (Kreiner 2004). The photoelectric observations in *BV* bands were obtained by Broglia & Conconi (1979). Based on normal points in *B* and *V* bands, they derived a detached configuration for an assumed mass ratio of 0.75 (Brancewicz & Dworak 1980). There exists a small seasonal change in the LCs between 1976 and 1977, whose intrinsic variability may be attributed to the activity in this binary.

In present work, two near-contact binaries (NCBs), IZ Mon and AR Dra, are photometrically observed. New photometric data are presented in Section 2. Orbital period studies and light-curve analyses are given in Sections 3 and 4. In the last section, we interpreted the period variations and discussed the possible evolutionary states of two systems.

2. OBSERVATIONS

CCD Photometry for IZ Mon and AR Dra, was acquired using the 60 cm telescope (Yang 2009) and the 85 cm telescope (Zhou et al. 2009) at the Xinglong station (XLs) of National Astronomical Observatories of China (NAOC). Two telescopes are equipped with the standard Johnson-Cousins $UBVR_cI_c$ filters. Data reduction was performed by the aperture photometry package IRAF in a standard fashion. We then obtained the individual observations as heliocentric Julian dates and differential magnitudes (i.e., HJD versus Δm), which are listed in Table 1.

The complete LCs for IZ Mon were obtained on 2009 January 20, 22, 24, 25, and 26, and March 1, using the 85 cm telescope. The comparison and check stars are TYC 748-849-1 and TYC 784-821-1, respectively. The exposure times are fixed to be 20, 15, and 15 s for *BVR* bands, respectively. The 1σ errors for the photometric bands are $\pm0^{m}.008$ in the *B* band, $\pm0^{m}.006$ in the *V* band, and $\pm0^{m}.005$ in the *R* band, respectively. A total of 961, 960, and 959 effective images in *BVR* bands are obtained. The differential LCs (i.e., LC_1) are displayed in Figure 1, in which phases are computed by a period of $0^{d}.7798076$ (Kreiner et al. 2001). From this figure, there exists an unequal height between both maxima of light. Max.I at phase 0.25 is brighter than Max.II at phase 0.75 up to $0^{m}.031$ in the *B* band, $0^{m}.027$ in the *V* band, and $0^{m}.025$ in *R* band, respectively. Moreover, another primary eclipse for IZ Mon was monitored on 2011 January 17.

Another binary AR Dra was observed on 2009 February 20, 25, 26, and 27, with the 65 cm telescope. TYC 4158-264-1 and TYC 4158-1275-1 are chosen to be the comparison and check stars. The typical exposure times are 50, 40 and 40 s for *BVR* bands, which depend on the condition of weather. In total, we obtained 733, 728 and 356 images in *B*, *V* and *R* bands, respectively. The standard deviation for individual points is less than 0.007 mag in three bands. The *BVR* LCs are shown in the left panel of Figure 2, whose phases are calculated by a period

Table 1
Photometric Observations for IZ Mon and AR Dra

Star	*B* band		*V* band		*R* band	
	JD(Hel.)	Δm	JD(Hel.)	Δm	JD(Hel.)	Δm
	2456882.95211	1.553	2456882.95239	1.416	2456882.95515	1.340
	2456882.95461	1.561	2456882.95322	1.427	2456882.95598	1.356
	2456882.95544	1.562	2456882.95489	1.433	2456882.95681	1.353
IZ Mon	2456882.95824	1.569	2456882.95572	1.419	2456882.95764	1.362
	2456882.96061	1.563	2456882.95654	1.430	2456882.95888	1.360
	2456882.96179	1.558	2456882.95858	1.429	2456882.96020	1.342
	2456882.96297	1.563	2456882.95983	1.430	2456882.96138	1.355
	2456883.15423	0.551	2456883.15699	0.702	2456883.15563	0.782
	2456883.15613	0.553	2456883.15894	0.704	2456883.15758	0.788
	2456883.15820	0.552	2456883.16086	0.702	2456883.15945	0.787
AR Dra	2456883.16003	0.557	2456883.16276	0.705	2456883.17868	0.801
	2456883.16195	0.560	2456883.16466	0.709	2456883.18253	0.808
	2456883.16390	0.559	2456883.16858	0.708	2456883.18450	0.810
	2456883.16584	0.564	2456883.17044	0.712	2456883.18633	0.812

(This table is available in its entirety in machine-readable form.)

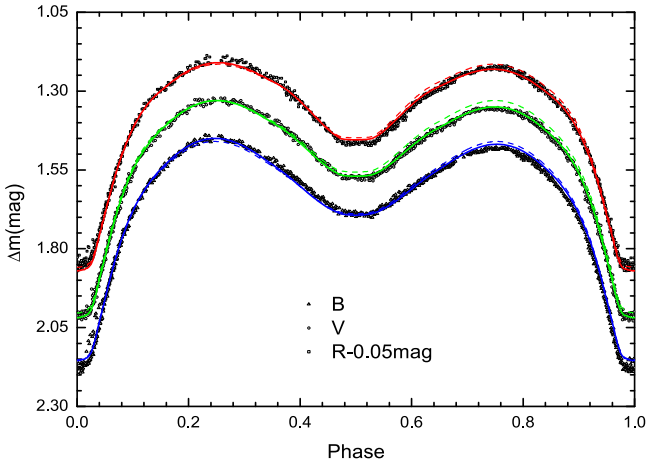

Figure 1. Photometric observations of IZ Mon, obtained in 2009 February and March. The solid and dotted lines are plotted by photometric solutions, Sol.1 and Sol.2 with a hot spot, respectively.

of $0\overset{d}{.}67583743$ (Kreiner et al. 2001). The variable light amplitudes are $1\overset{m}{.}44$, $1\overset{m}{.}27$, and $1\overset{m}{.}31$ for *B*, *V,* and *R* bands. The *BV*-band amplitudes are a bit larger than Broglia & Conconi's (1979) values of $1\overset{m}{.}22$ in the *B* band and $1\overset{m}{.}19$ in the *V* band, respectively.

3. ORBITAL PERIOD STUDIES

From our observations, several light minimum times for IZ Mon and AR Dra were determined by means of a parabolic fitting method. Table 2 tabulates these individual data and their errors. For IZ Mon and AR Dra, all available light minimum times are accumulated and listed in Tables 2 and 3, in order to study period variations. In the fitting process for the $(O - C)$ curves, weights 1 and 1000 are assigned to "p/vi/pg" and "pe/CCD" data[3] for the differential measured methods.

3.1. IZ Mon

From the early eclipsing times of IZ Mon, Wood & Forbes (1963) obtained a cubic ephemeris with period increasing. Due to short baseline and large noise for minimum times, this result did not reveal the true period changes. We collected 57 light minimum times, including 24 plate, 11 visual, 1 photographic, 3 photoelectric, and 19 CCD measurements. By using Kreiner et al.'s (2001) linear ephemeris,

$$\text{Min. I} = \text{HJD } 2427344.644 + 0.7798076 \times E, \qquad (1)$$

we then computed the initial residuals, $(O - C)_{\rm i}$, which are listed in Table 3, and shown in the upper panel of Figure 3. From this figure, a long gap occurs from 1950 to 2001, except for two data, i.e., HJD 2442450.298 (Diethelm 1975) and HJD 2447914.386 (Kohl 1990). However, there evidently exists a secular period decrease. A linear least-squares fitting method yields a quadratic ephemeris as follows,

$$\begin{aligned}\text{Min. I} = {} & \text{HJD } 2427344.6256(\pm 0.0048) \\ & + 0.77981286(\pm 0.00000008) \\ & \times E - 2.20(\pm 0.04) \times 10^{-10} \times E^2. \end{aligned} \qquad (2)$$

Table 3 lists the final timing residuals, $(O - C)_f$, which are also displayed in the lower panel of Figure 3. From the coefficient of the quadratic term of $Q = -2.20(\pm 0.04) \times 10^{-10}$, a long-term period continuously decreases at a rate of $dP/dt = 365.24 \times \frac{2Q}{P} = -2.06(\pm 0.04)$ days yr^{-1}, where P is the period of the binary in units of days. The calculated curve from Equation (2) is plotted as a solid line in its upper panel, which gives a good fit for data.

3.2. AR Dra

For another binary, AR Dra, we accumulated a total of 124 light minimum times (i.e., 14 plate, 70 visual, 13 photoelectric, and 27 CCD ones), which are listed in Table 3. With the

[3] Methods of "p," "vi," "pg," "pe," and "CCD" are plate, visual, photographic, photometric and charge-coupled device observations, respectively. The time of mid-exposure of a photographic plate (i.e., "p") was taken when the star was near minimum. Meanwhile, the "p" minima were obtained from a series of photographic data.

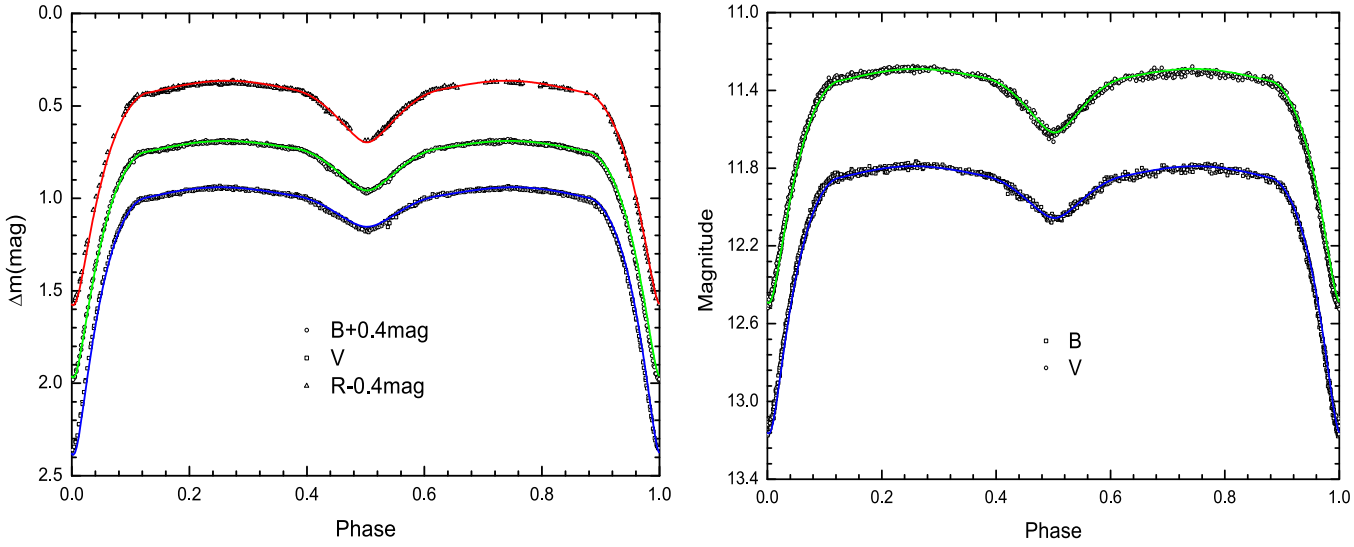

Figure 2. Left panel: multi-color light curves of AR Dra, observed in 2009 Febuary. Right panel: *BV* observations of Broglia & Conconi (1979). The solid lines are constructed by Sol.1 from LC_1 and Sol.2 from LC_2, respectively.

Table 2
New Observed Light Minimum Times

Star	JD(Hel.)	Error	Min.	Filter
	2454883.05944	±0.00031	II	*B*
	2454883.05833	±0.00034	II	*V*
	2454883.05714	±0.00035	II	*R*
	2454885.00282	±0.00024	I	*B*
	2454885.00286	±0.00022	I	*V*
	2454885.00278	±0.00023	I	*R*
	2454888.12146	±0.00013	I	*B*
IZ Mon	2454888.12100	±0.00018	I	*V*
	2454888.12101	±0.00019	I	*R*
	2454892.01756	±0.00030	I	*B*
	2454892.01970	±0.00027	I	*V*
	2454892.01914	±0.00043	I	*R*
	2455579.01360	±0.00020	I	*B*
	2455579.01666	±0.00018	I	*V*
	2455579.01683	±0.00021	I	*R*
	2454883.28906	±0.00019	I	*B*
	2454883.28900	±0.00044	I	*V*
	2454883.28936	±0.00017	I	*R*
	2454888.35922	±0.00024	II	*B*
	2454888.35921	±0.00024	II	*V*
AR Dra	2454889.37192	±0.00026	I	*B*
	2454889.37178	±0.00016	I	*V*
	2454889.37189	±0.00050	I	*R*
	2455579.01360	±0.00019	I	*B*
	2455579.01666	±0.00018	I	*V*
	2455579.01683	±0.00021	I	*R*

following linear ephemeris (Kreiner et al. 2001),

$$\text{Min. I} = \text{HJD } 2442868.9124 + 0.67583743 \times E, \quad (3)$$

one can compute the initial timing residuals, $(O - C)_i$, which are listed in Table 4, and shown in the upper panel of Figure 4. Considered a continuous period variation, the eclipse timing residuals were fitted by the following parabolic curve,

$$(O - C)_i = -0.0014(\pm 0.0006) - 6.36(\pm 0.15) \times 10^{-7} \times E + 9.49(\pm 1.18) \times 10^{-11} \times E^2. \quad (4)$$

Equation (2) is plotted as a dotted line in its upper panel. From this figure, the quadratic curve evidently deviates from the general trend. Therefore, we assumed the parabola of Equation (2) as a part of the sinusoidal curve. Using a nonlinear least-squared fitting method, we yielded the following formula,

$$(O - C)_i = +0.0097(\pm 0.0013) + 1.05(\pm 0.04) \times 10^{-7} \times E + 0.0196(\pm 0.0010) \times \sin[1.11(\pm 0.03) \times 10^{-4} \times E + 3.726(\pm 0.066)]. \quad (5)$$

After being removed from Equation (5), the final timing residuals, i.e., $(O - C)_f$, are listed in Table 4 and shown in the lower panel of Figure 4. In the upper panel of Figure 4, Equation (5), as a solid line, fits photoelectric/CCD data fairly well though the early low-precision data and the early timings have such large scatter. The modulated period for this oscillation is $P_3 = 104.9(\pm 2.9)$ yr, which is longer than the observed time span (i.e., ~80 yr). This case is similar to the previously studied binary WY Tau (Yang 2009). The true period variation for AR Dra may be needed to further check in the future.

4. PHOTOMETRIC SOLUTIONS

Multi-color LCs of IZ Mon and AR Dra were simultaneously analyzed by the 2015 version of the W-D program[4] (Wilson & van Hamme 2014), which can solve LCs, eclipse timings together (also velocities), including a third body light-time effect. Regrettably, no radial velocities for two binaries have been published up to now. So we indirectly have to determine

[4] Available at the website: ftp://ftp.astro.ufl.edu/pub/wilson/lcdc2015.

Table 3
Previously Published and New Eclipsing Times for IZ Mon

JD(Hel.)	Epoch	Method	Min	$(O-C)_i$ (days)	$(O-C)_f$ (days)	Ref.
2427344.593	+0.0	pv	I	−0.0510	−0.0326	(1)
2427344.621	+0.0	pg	I	−0.0230	−0.0046	(2)
2427369.542	+32.0	pv	I	−0.0558	−0.0375	(1)
2427416.423	+92.0	pv	I	+0.0367	+0.0547	(1)
2428074.559	+936.0	pv	I	+0.0151	+0.0288	(1)
2428213.285	+1114.0	pv	I	−0.0647	−0.0518	(1)
2428245.327	+1155.0	pv	I	+0.0052	+0.0179	(1)
2428428.610	+1390.0	pv	I	+0.0334	+0.0449	(1)
2428453.563	+1422.0	pv	I	+0.0326	+0.0440	(1)
2428542.453	+1536.0	pv	I	+0.0245	+0.0354	(1)
2428835.662	+1912.0	pv	I	+0.0259	+0.0351	(1)
2429168.592	+2339.0	pv	I	−0.0220	−0.0147	(1)
2429193.533	+2371.0	pv	I	−0.0348	−0.0276	(1)
2429229.480	+2417.0	pv	I	+0.0410	+0.0480	(1)
2430326.647	+3824.0	pv	I	+0.0187	+0.0202	(1)
2430372.573	+3883.0	pv	I	−0.0639	−0.0626	(1)
2430376.528	+3888.0	pv	I	−0.0079	−0.0066	(1)
2430380.384	+3893.0	pv	I	−0.0510	−0.0497	(1)
2430383.513	+3897.0	pv	I	−0.0412	−0.0399	(1)
2431435.552	+5246.0	pv	I	+0.0373	+0.0342	(1)
2431470.550	+5291.0	pv	I	−0.0560	−0.0592	(1)
2432175.528	+6195.0	pv	I	−0.0241	−0.0298	(1)
2432211.446	+6241.0	pv	I	+0.0228	+0.0170	(1)
2432884.436	+7104.0	pv	I	+0.0388	+0.0310	(1)
2432912.475	+7140.0	vi	I	+0.0047	−0.0032	(1)
2432944.459	+7181.0	vi	I	+0.0166	+0.0086	(1)
2432951.471	+7190.0	vi	I	+0.0104	+0.0024	(1)
2432969.406	+7213.0	vi	I	+0.0098	+0.0017	(1)
2432997.485	+7249.0	vi	I	+0.0157	+0.0076	(1)
2433001.371	+7254.0	vi	I	+0.0027	−0.0054	(1)
2433305.505	+7644.0	vi	I	+0.0117	+0.0028	(1)
2433348.388	+7699.0	vi	I	+0.0053	−0.0037	(1)
2433359.320	+7713.0	vi	I	+0.0200	+0.0110	(1)
2442450.2980	+19371.0	vi	I	+0.0010	+0.0000	(3)
2447914.3860	+26378.0	vi	I	−0.0229	+0.0097	(4)
2451965.4387	+31573.0	CCD	I	−0.0707	+0.0008	(5)
2452688.3091	+32500.0	CCD	I	−0.0819	−0.0023	(6)
2452992.820	+32890.5	CCD	II	−0.0859	−0.0027	(7)
2453056.3761	+32972.0	CCD	I	−0.0841	−0.0001	(5)
2453768.334	+33885.0	CCD	I	−0.0905	+0.0021	(7)
2453814.3397	+33944.0	CCD	I	−0.0935	−0.0004	(8)
2453846.3090	+33985.0	CCD	I	−0.0963	−0.0028	(8)
2454148.0958	+34372.0	CCD	I	−0.0950	+0.0023	(9)
2454172.2683	+34403.0	CCD	I	−0.0966	+0.0010	(8)
2454513.4324	+34840.5	CCD	II	−0.0983	+0.0037	(10)
2454883.0583	+35314.5	CCD	II	−0.1012	+0.0056	(11)
2454885.0028	+35317.0	CCD	I	−0.1062	+0.0006	(11)
2454888.1212	+35321.0	CCD	I	−0.1070	−0.0001	(11)
2454892.0188	+35326.0	CCD	I	−0.1085	−0.0016	(11)
2455236.3007	+35767.5	pe	II	−0.1116	−0.0001	(12)
2455259.3045	+35797.0	CCD	I	−0.1122	−0.0004	(13)
2455579.0157	+36207.0	CCD	I	−0.1221	−0.0060	(11)
2455599.2970	+36233.0	pe	I	−0.1158	+0.0006	(13)
2455620.3513	+36260.0	CCD	I	−0.1163	+0.0004	(13)
2455623.4724	+36264.0	pe	I	−0.1144	+0.0023	(12)
2455629.3188	+36271.5	CCD	II	−0.1166	+0.0002	(13)
2455956.4406	+36691.0	CCD	I	−0.1241	−0.0028	(13)

References. (1) Hoffmeister (1954), (2) Hoffmeister (1952), (3) Diethelm (1975), (4) Kohl (1990), (5) Zejda (2004), (6) Agerer & Hübscher (2003), (7) Hübscher (2007), (8) Brát et al. (2007), (9) Nagai (2008), (10) Hübscher et al. (2009), (11) Present work, (12) Hübscher et al. (2012), (13) Brát et al. (2011).

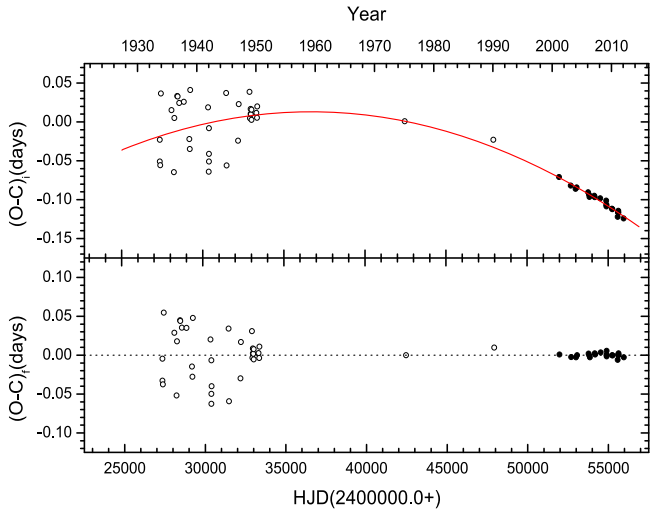

Figure 3. Timing residual curves for IZ Mon. The open circles refer to photographic observations, while the solid circles do photoelectric and CCD ones, respectively. Equation (2) is plotted as a solid line.

absolute parameters from spectral type or color index. The mass ratios were searched from LCs. Certainly, the validity of solutions are identified by radial velocity curves for two binaries. The gravity-darkening exponents, $g = 4\beta$, are adopted to be 1.0 for stars with radiative envelopes (von Zeipel 1924) and 0.32 for stars with convective envelopes (Lucy 1967). The logarithmic limb-darkening coefficients are interpolated into the tables of van Hammme (1993). The adjustable parameters are i, q, T_2, Ω_1, L_1, or L_2.

4.1. IZ Mon

From the 2MASS survey (Cutri et al. 2003), the color index is $J - H = +0.037(\pm 0.024)$, approximately corresponding to a spectral type of $A2/3$ (Cox 2000). Therefore, we adopted an effective temperature of $T_1 = 8500(\pm 210)$K for the primary component. We began the LC fitting experiments in Mode 2, but found that a semi-detached configuration with the primary filling its Roche lobe (i.e., Mode 4). A series of tried solutions were carried out for some fixed mass ratios from 0.34 to 0.70. The resulting relation between $\Sigma(o-c)_i^2$ (i.e., the resulting sum of weighted square deviations) and q is plotted in the left panel of Figure 5. We reached the minimum residuals at $q = 0.38$, which is then taken as an initial value for modeling LCs. After some iterations, we obtained the photometric solution (i.e., Sol.1), which is listed in Table 5. From Figure 1, there exists a small hump in the first maxima, which may result from magnetic activity of the cool component or mass transfer from the primary component. In the following section, we calculated the mean subsurface magnetic field strength of $B_2 = 58.0(\pm 1.5)$ kG (seen from the mechanism of magnetic activity in Section 5). So we remove this mechanism. Then we assumed a hot spot on the equator of the secondary's surface (i.e., the colatitude of $\phi = 90°$). The free parameters are extended to include the mass ratio of q, and the other three hot spot parameters (i.e., longitude θ, angular radius γ, and temperature factor T_s/T). We then derived the final photometric elements (i.e., Sol.2), which are given in Table 5. As illustrated in Figure 1, the theoretical LCs are computed from Sol.1 and Sol.2 as solid and dotted lines. There exists a small scatter of occuring LCs in B and R bands, which may result from the simultaneous solution from three bands. The asymmetrical LCs may result from mass transfer from the hot component through the inner Langrangian point onto the surface of the cool component, and thus it causes additional light near phase 0.25 (Shaw 1994). This case occurs in other NCBs, such as, BL And (Zhu & Qian 2006) and GO Cyg (Ulaş et al. 2012).

4.2. AR Dra

From the BV LCs (i.e., LC_2), Broglia & Conconi's (1979) suggested that AR Dra is a detached binary. It may be unreliable to assume a mass ratio of 0.75 from seasonal normal points. This situation occurs in another previously studied binary FR Ori (Yang et al. 2014). Based on its spectral type of F5V, the mean effective temperature of Star 1 was adopted as $T_1 = 6550$ K (Harmanec 1988). The "q-search" process was performed from our BVR observations (i.e., LC_1) and Broglia & Conconi's (1979) data (i.e., LC_2), respectively. The tried solutions identified that AR Dra is a detached binary. The $q - \Sigma$ curves are shown in Figure 5, in which the minimum values of $\Sigma(o-c)_i^2$ are achieved around $q = 0.65$. Finally, we derived two sets of photometric elements (i.e., Sol.1 from LC_1 and Sol.2 from LC_2), which are listed in Table 5. Figure 2 displays the computed LCs as solid lines, which give good fits for observations. The mass ratio of $q_{\rm ph} = 0.652(\pm 0.002)$ is smaller than the assumed value of 0.75 (Broglia & Conconi 1979). The inner critical potentials are $\Omega_{\rm in} = 3.1578$ at $q = 0.652$ from LC_1 and $\Omega_{\rm in} = 3.1632$ at $q = 0.655$ from LC_2, respectively. From Table 5, the modified dimensionless surface potential, $\Omega_{1,2}$, is larger than, or near to, the inner critical potential. Therefore, the primary component lies inside its Roche lobe, while the secondary component is near its Roche lobe.

5. DISCUSSIONS

From the spectral type of F5V for AR Dra (assumed with an error of a subclass), the mass of the primary is adopted to be $M_1 = 1.31(\pm 0.03)\,M_\odot$ (Harmanec 1988). Meanwhile, the primary's mass of $M_1 = 2.01(\pm 0.06)\,M_\odot$ for IZ Mon is estimated from its color index of $J - H$. The bolometric luminosity for the component is $L \propto R^2\,T^4$. By the aid of photometric elements, we approximately determined other absolute parameters, which are listed in Table 6. The mass–luminosity diagram for NCBs is shown in Figure 6, in which the zero-age main sequence (ZAMS) and terminal-age main sequence (TAMS) lines are plotted by the binary-star evolution code (Hurley et al. 2002). Two components for AR Dra is located above the ZAMS line. While, both components for IZ Mon lie around the ZAMS line. This implies that IZ Mon may be situated at the semi-detached stage of the thermal relaxation oscillation (Lucy 1976; Robertson & Eggleton 1977; Webbink 2003).

Given the non-conservative evolution, the period changes for close binaries should generally result from the net effect of mass transfer between components, mass loss, and angular momentum loss by magnetic stellar wind. Tout & Hall (1991) gave the following relation,

$$\frac{\dot{P}}{P} = -\frac{2\dot{M}}{M} + \frac{3(M_2 - M_1)}{M_1 M_2}\dot{M}_2 + 3 \times \frac{2}{3}\left(\frac{R_A}{a}\right)^2 \frac{M}{M_1 M_2}\dot{M}, \quad (6)$$

Table 4
Previously Published and New Light Minimum Times for AR Dra

JD(Hel.)	Epoch	Method	Min	$(O-C)_i$ (days)	$(O-C)_f$ (days)	Ref.
2426751.541	−23848.0	p	I	−0.0004	−0.0023	(1)
2426808.352	−23764.0	p	I	+0.0403	+0.0383	(1)
2428246.507	−21636.0	p	I	+0.0132	+0.0073	(1)
2428248.507	−21633.0	p	I	−0.0143	−0.0202	(1)
2428636.439	−21059.0	p	I	−0.0130	−0.0198	(1)
2428684.432	−20988.0	p	I	−0.0044	−0.0113	(1)
...	...					
2455615.9028	+18861.0	CCD	I	+0.0206	−0.0001	(61)
2455684.8380	+18963.0	CCD	I	+0.0204	−0.0006	(61)
2455314.4779	+18415.0	pe	I	+0.0192	−0.0002	(62)
2455980.8543	+19401.0	CCD	I	+0.0199	−0.0025	(63)
2456045.7398	+19497.0	CCD	I	+0.0250	+0.0023	(63)
2456297.1506	+19869.0	CCD	I	+0.0243	+0.0005	(64)

References. (1) Strohmeier (1959a), (2) ....., (61) Diethelm (2011), (62) Hübscher et al. (2012), (63) Diethelm (2012), (64) Nagai (2014).
(This table is available in its entirety in machine-readable form.)

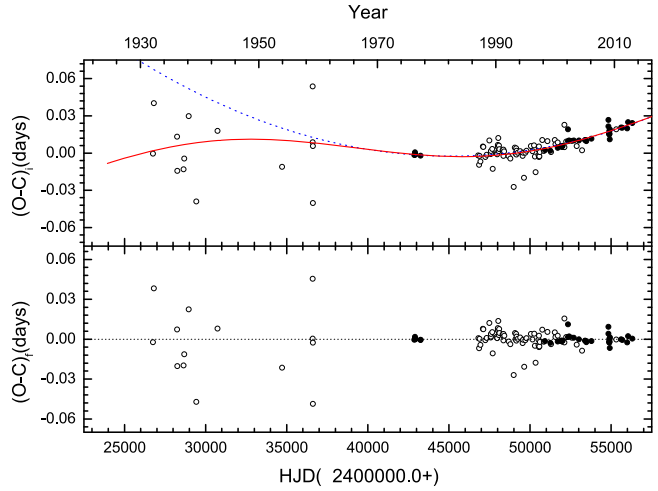

Figure 4. Eclipse timing residual diagrams of AR Dra. Two possible period variations are described by the dotted and solid lines from Equations (4) and (5), respectively. Other symbols are the same as in Figure 3.

where R_A, a, and $M$are the Alfvén radius, the separation between both components, and the total mass of the binary system. Three terms of Equation (6) represent mass loss, mass transfer, and angular momentum loss, respectively. Considering the primary fills its Roche lobe for IZ Mon, $\dot{M}_2$ in the second term is replaced by $-\dot{M}_1$. Assumed $\dot{M}/M = \dot{M}_1/M_1$ and $R_A \simeq a$, Equation (6) may be simplified into the following formula,

$$\frac{\dot{P}}{P} = \frac{2q^2 - q + 5}{q}\frac{\dot{M}_1}{M_1}. \quad (7)$$

Inserting the related parameters of $\dot{P}$, M_1, q, and P into Equation (7), we can compute the mass-loss rate of $\dot{M}_1 = -3.27(\pm 0.10) \times 10^{-8}\, M_\odot\ \mathrm{yr}^{-1}$. With the period decreasing, the orbit will be shrinking. If two components are close enough to come into contact, IZ Mon will become an A-type W UMa system (Bradstreet & Guinan 1994).

For the previous analyses, AR Dra is a detached NCB, whose components do not fill their Roche lobes. Three mechanisms of Equation (6) could not cause the orbital period to increase. Therefore, it is acceptable for the cyclic variation to fit the $(O-C)$ curve. For the late-type binary, the magnetic activity cycles of one or two components may result in the observed oscillations (Applegate 1992). The variations of the gravitational quadrupole moment are computed by a relation of $-9\left(\left(\frac{R}{a}\right)^2 \frac{\Delta Q}{MR^2}\right) \simeq A\frac{2\pi P}{P_{\mathrm{mod}}}$ (Lanza & Rodonò 2002). The values are $\Delta Q_1 = 7.92(\pm 0.40) \times 10^{50}\ \mathrm{g\ cm^2}$ $\Delta Q_2 = 5.17(\pm 0.26) \times 10^{50}\ \mathrm{g\ cm^2}$, which are smaller than the typical order of 10^{51}–10^{52} for close binaries (Lanza & Rodonò 1999). The mean subsurface magnetic field strengths are $B_1 = 83.0(\pm 2.1)$ kG and $B_2 = 58.0(\pm 1.5)$ kG, which are evidently larger than the typical value, i.e., several kGs (Lanza & Rodonò 2002). Then, the cyclic magnetic activity of both components may not work, which results in the small hump of LCs. Therefore, Applegate's (1992) mechanism may become invalid in this system.

Another possible mechanism is light-time orbit effect due to the third body (Irwin 1952). By the known equation,

$$f(m) = \frac{(M_3 \sin i')^2}{(M_1 + M_2 + M_3)^3} = \frac{4\pi^2}{GP_3} \times (a_{12} \times \sin i') \quad (8)$$

we can calculate its mass function of $f(m) = 3.55(\pm 0.54) \times 10^{-3}\, M_\odot$ with $a_{12} \sin i' = A \times c = 3.39$ (± 0.17) au. The minimum mass for the additional companion is $M_3 = 0.28(\pm 0.02)\, M_\odot$ (at $i' = 90°$), which corresponds to a spectral type of M3 (Harmanec 1988). The light-time effect is accompanied by changes of the systemic radial velocity of the eclipsing pair. Its semi-amplitude can be computed by the following equation (Mayer 1990),

$$K_{V_r} = \frac{A}{P_3}\frac{5156}{\sqrt{(1-e^2)(1-e^2\cos^2\omega)}}, \quad (9)$$

where K_{V_r}, A, and P_3 are in $\mathrm{km\ s^{-1}}$, days, and years, respectively. Using the fitted parameters of Equation (5), we can obtain the value of $K_{V_r} = 0.96(\pm 0.08)\ \mathrm{km\ s^{-1}}$, which is sufficiently large for the present-day spectroscopy to reliably resolve. This may provide the existence of a tertiary companion through observing the variation of the systemic velocity of the

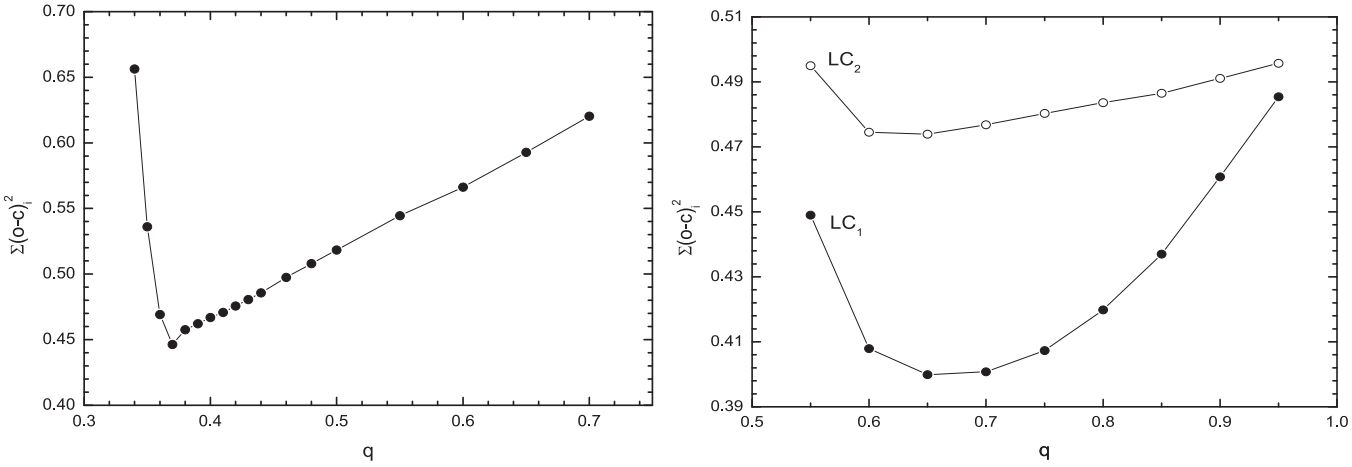

Figure 5. Resulting curves of $\Sigma(q)$ for IZ Mon (left panel) and AR Dra (right panel).

Table 5
Model Parameters for IZ Mon and AR Dra

Parameter	IZ Mon (Mode 4)		AR Dra (Mode 2)	
	Sol.1 (no spot)	Sol.2 (with spot)	Sol.1 from LC_1	Sol.2 from LC_2
$q = M_2/M_1$	0.380(±0.001)	0.388(±0.002)	0.652(±0.002)	0.655(±0.002)
i(°)	84.67(±0.10)	84.50(±0.07)	84.30(±0.05)	83.20(±0.06
T_1(K)	8500		6550	
Ω_1	2.6730	2.6535	3.6148(±0.0049)	3.8698(±0.0093)
X_1, Y_1	+0.676, +0.211		+0.645, +0.241	
x_{1B}, y_{1B}	+0.778, +0.379		+0.802, +0.256	
x_{1V}, y_{1V}	+0.686, +0.319		+0.709, +0.285	
x_{1R}, y_{1R}	+0.563, +0.260		+0.617, +0.285	…
T_2(K)	5120(±19)	4971(±15)	4863(±4)	5057(±6)
Ω_2	2.6690(±0.0051)	2.7058(±0.0039)	3.2188(±0.0026)	3.2289(±0.0041)
X_2, Y_2	+0.649, +0.180	+0.647, +0.172	+0.638, +0.152	+0.645, +0.165
x_{2B}, y_{2B}	+0.849, +0.061	+0.849, +0.033	+0.845,−0.058	+0.849, +0.006
x_{2V}, y_{2V}	+0.787, +0.167	+0.790, +0.144	+0.795, +0.071	+0.793, +0.123
x_{2R}, y_{2R}	+0.699, +0.208	+0.704, +0.194	+0.717, +0.150	…
$L_1/(L_1+L_2)_B$	0.9800(±0.0007)	0.9839(±0.0005)	0.8848(±0.0010)	0.8297(±0.0023)
$L_1/(L_1+L_2)_V$	0.9600(±0.0009)	0.9663(±0.0006)	0.8294(±0.0015)	0.7638(±0.0025)
$L_1/(L_1+L_2)_R$	0.9367(±0.0011)	0.9446(±0.0009)	0.7827(±0.0014)	…
R_1/a*(pole)	0.4368(±0.0003)	0.4351(±0.0003)	0.3339(±0.0005)	0.3084(±0.0009)
R_1/a(point)	0.5978(±0.0008)	0.5958(±0.0006)	0.3694(±0.0008)	0.3319(±0.0012)
R_1/a(side)	0.4666(±0.0004)	0.4646(±0.0003)	0.3450(±0.0006)	0.3164(±0.0010)
R_1/a(back)	0.4931(±0.0004)	0.4912(±0.0003)	0.3579(±0.0007)	0.3254(±0.0011)
R_2/a(pole)	0.2729(±0.0016)	0.2703(±0.0012)	0.3117(±0.0005)	0.3126(±0.0008)
R_2/a(point)	0.3510(±0.0077)	0.3372(±0.0042)	0.3896(±0.0020)	0.3912(±0.0033)
R_2/a(side)	0.2837(±0.0019)	0.2805(±0.0013)	0.3247(±0.0006)	0.3256(±0.0010)
R_2/a(back)	0.3127(±0.0030)	0.3071(±0.0022)	0.3518(±0.0009)	0.3529(±0.0015)
ϕ(°)	…	90	…	…
θ(°)	…	88.8(±3.1)	…	…
γ(°)	…	20.1(±1.2)	…	…
T_s/T	…	1.43(±0.2)	…	…

Note. * "a" refers to the separation between both components.

Table 6
Estimated Absolute Parameters for IZ Mon and AR Dra

Star	Separation	Primary Component			Secondary Component		
	$a(R_\odot)$	$M_1(M_\odot)$	$R_1(R_\odot)$	$L_1(L_\odot)$	$M_2(M_\odot)$	$R_2(R_\odot)$	$L_2(L_\odot)$
IZ Mon	5.22(±0.05)	2.01(±0.06)	2.48(±0.13)	28.7(±2.9)	0.78(±0.02)	1.49(±0.09)	1.22(±0.14)
AR Dra	4.19(± 0.03)	1.31(±0.03)	1.47(±0.05)	3.58(±0.24)	0.85(±0.02)	1.44(±0.05)	1.04(±0.07)

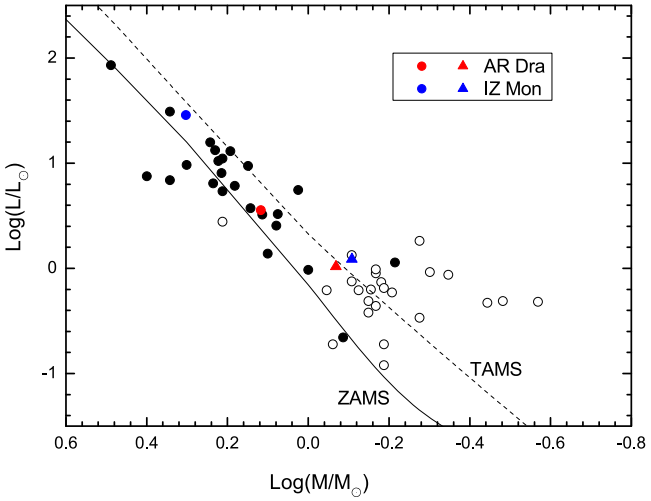

Figure 6. *M–L* diagram for the NCBs, where black symbols refer to NCBs from Yakut & Eggleton (2005). The open and filled circles represent the secondary and primary components. The ZAMS and TAMS are the continuous and dotted lines, respectively.

binary due to the reflex motion. Moreover, the additional companion may extract angular momentum from the central system. With two components evolving, they will fill their Roche lobes. Finally, these kinds of binaries, such as AR Dra, will come into contact through magnetic braking. In future work, high-precision spectroscopy and photometry for two binaries are needed in order to obtain radial velocities and new LCs, so we can determine the absolute parameters and identify the period variations.

The authors would like to express many thanks to the anonymous referee for invaluable comments. This research is supported by the Natural Science Foundation of China (grant Nos. 11473009 and U1131102), and the Open Research Program of Key Laboratory for the Structure and Evolution of Celestial Objects (No. OP201407). Dr. Y.-G. Yang acknowledges Professor J.-M. Kreiner for his compiled eclipsing times. New photometry of two objects was allowed to use the 60 and 85 cm telescopes at the XLs of NAOC.

REFERENCES

Agerer, F., & Hübscher, J. 2003, IBVS, 5484, 1
Applegate, J. H. 1992, ApJ, 385, 621
Bradstreet, D. H., & Guinan, E. F. 1994, in ASP Conf. Ser. 56, Interacting Binary Stars: A Symposium Held in Conjunction with the 105th Meeting of the Astronomical Society of the Pacific, ed. A. W. Shafter (San Francisco, CA: ASP), 228
Brancewicz, H. K., & Dworak, T. Z. 1980, AcA, 30, 501
Brát, L., Trnka, J., Smelcer, L., et al. 2011, OEJV, 137, 1
Brát, L., Zejda, M., & Svoboda, P. 2007, OEJV, 74, 1
Broglia, P., & Conconi, P. 1979, A&AS, 37, 487
Cox, A. N. (ed.) 2000, Allen's Astrophysical Quantities (4th ed.; New York: Springer)
Cutri, R. M., Skrutskie, M. F., van Dyk, S., et al. 2003, MASS All Sky Catalog of point sources, The IRSA 2MASS All-Sky Point Source Catalog, NASA/IPAC Infrared Science Archive, http://irsa.ipac.caltech.edu/applications/Gator
Diethelm, R. 1975, BBSAG, 21, 1
Diethelm, R. 2011, IBVS, 5992, 2
Diethelm, R. 2012, IBVS, 6029, 2
Harmanec, P. 1988, BAICz, 39, 329
Hill, G., Hilditch, R. W., Younger, F., & Fisher, W. A. 1975, MmRAS, 79, 131
Hoffmeister, C. 1944, AN, 274, 176
Hoffmeister, C. 1952, MVS, 1, 154
Hoffmeister, C. 1954, MiSon, 2, 43
Hübscher, J. 2007, IBVS, 5802, 1
Hübscher, J., Lehmann, P. B., & Wlater, F. 2012, IBVS, 6010, 1
Hübscher, J., Steinbach, H.-M., & Walter, F. 2009, IBVS, 5874, 1
Hurley, J. R., Tout, C. A., & Plos, O. R. 2002, MNRAS, 329, 897
Irwin, J. B. 1952, ApJ, 116, 211
Kinnunen, T., & Skiff, B. A. 2000, IBVS, 4879, 1
Koch, R. H. 1974, AJ, 79, 34
Kohl, M. 1990, BBSAG, 94, 1
Kreiner, J. M. 2004, AcA, 54, 207
Kreiner, J. M., Kim, C.-H., & Nha, I.-S. 2001, An Atlas of O-C Diagrams of Eclipsing Binary Stars (Kraków: Wydawnictwo Naukowe AP)
Kukarkin, B. V., Kholopov, P. N., Pskovsky, Y. P., et al. 1971, General Catalogue of Variable Stars (3rd ed.; Moskva: Astronomical Council of the Academy of Sciences in the USSR)
Lanza, A. F., & Rodonò, M. 1999, A&A, 349, 887
Lanza, A. F., & Rodonò, M. 2002, AN, 323, 424
Lucy, L. B. 1967, ZA, 65, 89
Lucy, L. B. 1976, ApJ, 205, 208
Mayer, P. 199, BAICz, 41, 231
Nagai, K. 2008, Var. Star Bull. Japan, 46, 1
Nagai, K. 2014, Var. Star Bull. Japan, 56, 1
Robertson, J. A., & Eggleton, P. P. 1977, MNRAS, 179, 359
Shaw, J. S. 1994, MmSAI, 65, 95
Strohmeier, W. 1959a, Kleine Veröff. Bamberg, 24, 1
Strohmeier, W. 1959b, Mitt. Veränd. Bd, 3, 1
Tout, C. A., & Hall, D. S. 1991, MNRAS, 253, 9
Ulaş, B., Kalomeni, B., Keskin, V., et al. 2012, NewA, 17, 296
van Hammme 1993, AJ, 106, 2096
von Zeipel, H. 1924, MNRAS, 84, 665
Webbink, R. F. 2003, ASPC, 297, 76
Wilson, R. E., & van Hamme, W. 2014, ApJ, 780, 151
Wood, B. D., & Forbes, J. E. 1963, AJ, 68, 257
Yakut, K., & Eggleton, P. P. 2005, ApJ, 629, 1055
Yang, Y.-G. 2009, PASJ, 61, 1211
Yang, Y.-G., Wei, J.-Y., & Li, H.-L. 2014, AJ, 147, 145
Zejda, M. 2004, IBVS, 5583, 1
Zhou, A.-Y., Jiang, X.-J., Zhang, Y.-P., & Wei, J.-Y. 2009, RAA, 9, 349
Zhu, L.-Y., & Qian, S.-B. 2006, MNRAS, 367, 423